Tailoring $Ca_3Co_4O_9$ microstructure and performances using a transient liquid phase sintering additive

A. Sotelo[a,*], F. M. Costa[b], N. M. Ferreira[b], A. Kovalevsky[c], M. C. Ferro[c], V. S. Amaral[d], J. S. Amaral[d], Sh. Rasekh[a], M. A. Torres[a], M. A. Madre[a], J. C. Diez[a]

[a]ICMA (CSIC-Universidad de Zaragoza), C/Maria de Luna, 3, 50018 Zaragoza, Spain.

[b]i3N, Physics Department, University of Aveiro, Aveiro, 3810-193, Portugal.

[c]CICECO–Aveiro Institute of Materials, Department of Materials and Ceramic Engineering, University of Aveiro, 3810-193 Aveiro, Portugal.

[d]CICECO–Aveiro Institute of Materials, Physics Department, University of Aveiro, 3810-193 Aveiro, Portugal.

Abstract

A flexible, adaptable, economical and easily scalable processing route, allowing microstructural control, is presented. It involves classical solid state sintering method and addition of liquid promoting compound. Controlled porosity and high thermoelectric performance have been attained in $Ca_3Co_4O_9$ by K_2CO_3 additions, drastically improving the sintering procedure. K_2CO_3 behaves as transient liquid phase, providing microstructural benefits, vanishing during sintering. Electrical resistivity was improved by enhanced grains connectivity and growth. Significant increase in Seebeck coefficient at high temperatures has been produced while lattice thermal conductivity was unaffected. The best ZT value, estimated at 800 ºC, assuming the thermal conductivity value at 140 ºC, is 0.35 for 5 wt.% K_2CO_3 samples. These values are significantly higher than that obtained for highly-dense textured materials at the same temperature.

The results suggest that this approach is very effective for preparing highly-performing $Ca_3Co_4O_9$-based thermoelectric materials with relatively high porosity to control thermal conductivity.

Keywords: Sintering; Microstructure-final; Electrical properties; Thermopower; ZT

Corresponding Author

* M. A. Madre. +34 976 762617

ICMA (CSIC-Universidad de Zaragoza), C/Maria de Luna, 3, 50018 Zaragoza, Spain. amadre@unizar.es.

1. Introduction

Since the discovery of promising thermoelectric (TE) properties in $NaCo_2O_4$ ceramics [1], with the ability to operate at high temperatures under air atmosphere without degradation, many works have been focused on this Co-based TE family. Those intense studies resulted in the discovery of new cobalt oxide-based thermoelectrics, which today are an important subject of research [2,3]. The performance of these thermoelectric materials is usually evaluated through the dimensionless figure of merit, ZT ($=S^2T/\rho\kappa$), where S, T, ρ, and κ are Seebeck coefficient, absolute temperature, electrical resistivity, and thermal conductivity, respectively. As bulk materials, these oxides usually demonstrate quite low thermoelectric performance, which make them no feasible for any practical applications. Envisaging the increment of ZT, many processing and structural engineering routes were attempted, including cationic substitution in solid state sintered materials [4,5], or taking advantage of their crystallographic nature to align the grains into a preferential direction using well-known techniques such as templated grain growth (TGG) [6], hot-pressing [7], spark plasma sintering (SPS) [8], laser floating zone (LFZ) [9], or the recently developed electrically assisted laser floating zone (EALFZ) [10]. These texturing techniques have been reported to produce bulk high density materials with well oriented grains, leading to enhanced electrical conductivity.

An important discovery from all these studies is the fact that, indeed, new preparation routes allow a significant increase in the thermoelectric performance, while the coupling between electrical and thermal properties can also be overcome. These methods aim at decreasing the electrical resistivity and thermal conductivity, while increasing, or maintaining practically constant,

Seebeck coefficient. Consequently, in these materials good grain connectivity should be obtained to improve electrical conductivity without drastically modifying S. Moreover, a relatively high porosity to decrease thermal conductivity of the bulk material is also favourable. The formation of strong grain boundaries has been already successfully achieved in several ceramic materials, by the formation of liquid phase, promoted by metallic Ag addition to the bulk material [11,12]. In the case of $Ca_3Co_4O_9$ ceramic materials, it is essential to find an additive compatible with this phase, with a melting point close to the sintering temperature, and which is not reacting with any one of the matrix components. In the literature, many examples of these kind of materials can be found as part of the fluxes used to grow $Ca_3Co_4O_9$ single crystals [13,14]. Among these materials, K_2CO_3 possess melting point (899 ºC) [15] very close to the optimal $Ca_3Co_4O_9$ materials sintering temperature, as reported in previous works [16]. Furthermore, these studies have shown that K_2CO_3 has not a detrimental effect on the thermoelectric performances of single crystals. Herein, a very facile and scalable sintering method for producing highly-performing and relatively porous $Ca_3Co_4O_9$ thermoelectric ceramics has been developed. The effect of relatively small additions of K_2CO_3, as liquid phase promoter during the sintering process, to the thermoelectric $Ca_3Co_4O_9$ bulk ceramics has been studied in this work. The structural and microstructural features are related with the thermoelectric properties.

2. Experimental

Polycrystalline $Ca_3Co_4O_9$ samples, pure and containing 5 and 10 wt.% K_2CO_3, were prepared by the classical solid state route from $CaCO_3$ (≥ 99%, Aldrich),

Co_3O_4 (99.5%, Panreac), and K_2CO_3 (≥ 99%, Aldrich) commercial powders. After mixing in stoichiometric proportions, the precursors were milled in aqueous media in an agate ball mill for 30 min at 300 rpm. The resulting suspension was then collected and completely dried using a rapid infrared evaporation system. This adjusted procedure allows very fine distribution of K_2CO_3 particles in the resulting precursor powder after evaporation of the solvent, provided by the high solubility of potassium carbonate in water and rapid drying. The dry powdered mixtures were annealed at 750 and 800 ºC for 12 h, with an intermediate manual grinding, to decompose $CaCO_3$, as reported in previous works [17]. The resulting powder was uniaxially compacted at ~ 400 MPa in form of pellets (around 3 mm X 3 mm X 14 mm), followed by sintering at 900 ºC for 24 h. During the sintering step the samples were horizontally placed on an alumina powder bed.

Phases in sintered materials were identified by powder X-ray diffraction (XRD) analysis, using a Rigaku D/max-B X-ray powder diffractometer (CuKα radiation) with 2θ ranging between 10 and 60 degrees. Microstructural observations and comparative analysis of element distribution were performed on longitudinal polished sections of samples in a FESEM (Zeiss Merlin), equipped with an energy dispersive spectrometry (EDS) system (INCA 350, Oxford Instruments). Additional HRTEM (JEOL model JEM-2200FS) studies of the 5 wt. % K_2CO_3 samples were conducted to identify the structural features, with emphasis on possible effects provided by potassium ions. Apparent density was measured using Archimedes' principle for each composition, at least for four ceramic samples, and compared to the theoretical density (4.677 g/cm^3) [18].

Electrical resistivity and Seebeck coefficient were simultaneously measured for all samples, using the steady state mode, by the standard DC four-probe technique in a LSR-3 apparatus (Linseis GmbH) in the range from 50 to 800 ºC under He atmosphere. Thermoelectric performance was evaluated and compared through the power factor, as $PF=S^2/\rho$. Thermal conductivity measurements were performed at 25-140 ºC, using a transient plane source technique (Hot Disk TPS 2500 s). This method involves an electrically conducting pattern element, acting both as a temperature sensor and heat source, insulated with two thin layers of Kapton (70 μm). The TPS element is sandwiched between two similar samples, with both faces being in contact with the samples surfaces. The measurements were performed using heating power from 7 to 9 W and measurement time from 20 to 80 s. ZT values were calculated at 25-140 ºC, based on the data of power factor and thermal conductivity. As the thermal conductivity of $Ca_3Co_4O_9$–based material is known to decrease on heating [19,20], with relatively weak temperature dependence at T > 200-300 ºC, the ZT values have been estimated at higher temperatures and compared to the best up-to-date literature data.

3. Results and discussion

A simplified sketch of the expected sintering mechanism is given in Fig. 1. Heating of the prepared compacts up to 900 ºC is accompanied by the formation of liquid K_2CO_3 phase, coexisting with solid calcium cobaltite grains. Classical mechanism of the liquid phase sintering involves wetting of the solid phase, penetration of the liquid into the pores, driven by an interplay between capillary forces, viscosity and gravity, rearrangement of the grains to closer

packing and progressive annihilation of pores [21], resulting in the material densification and rigid bonding between the grains. Partial solution of the matrix material in the melt and softening of the solid phase, provided by appropriate treatment conditions, can further assist the densification. In classical approach, on cooling the liquid solidifies to form a composite microstructure with tailored properties.

An interesting feature of the prepared materials refers to the chemical composition at the microscale level. According to the results of detailed SEM/EDS studies performed on sintered fractured and polished ceramics, the potassium concentration, both at the grain boundaries and in intragranular space, was below the detection limit of the equipment, roughly 0.1 % mass concentration. Although one should not completely exclude possible presence of potassium impurities, additional TEM imaging confirms compositional homogeneity of the samples. A representative TEM micrograph, showing typical grain boundaries and corresponding EDS mapping results, are presented in Fig. 2. The nominal composition of this sample corresponds to 5 wt.% of K_2CO_3, which is fairly above the EDS detection limit for potassium cations.

Among the factors which facilitate vanishing of the liquid phase, at least, it can be considered partial volatilization of K_2CO_3 under sintering conditions. The literature data suggest significant weight losses for K_2CO_3 even below melting point, mainly provided by decomposition reaction and partially due to congruent sublimation process [22]. Potassium oxide, as a product of decomposition, could easily react with moisture traces to produce KOH. Moreover, under discussed sintering conditions, potassium carbonate itself can undergo the hydrolysis reaction. In general, volatilization of the molten K_2CO_3 is known as

one the factors that limit the performance of molten carbonate fuel cells (MCFC), even operating at lower temperatures [23]. The carbonate losses in this case are further facilitated by the presence of water traces, due to the formation of alkali hydroxides, which have a vapor pressure of about an order of magnitude higher than the corresponding carbonates.

On the other hand, as sintered materials still possess a noticeable level of porosity as will be discussed below, the melt can be also forced to flow downwards against the capillary forces under the gravity effect, and infiltrate into the alumina powder bed, used as a support. This might also contribute as a plausible explanation for the transient behaviour of the liquid phase during sintering. In order to verify this hypothesis, the alumina bed where a bar-shaped sample was sintered in a horizontal position was analysed by SEM/EDS, Fig. 3. Three visually distinct regions, including the one beneath the sample (right side of Fig. 3a), were further analysed by EDS in selected areas. The results, presented in Fig. 3b and Table 1, clearly confirm presence of potassium in the alumina bed, with decreasing concentration when the distance from the sample is raised. At the same time, no signs of calcium and/or cobalt diffusion into the alumina bed were observed. It should be highlighted that prevailing mechanism for potassium depletion might still be based on the volatilization losses, as it can also result in the enrichment of the alumina bed with potassium.

These results, as a whole, indicate that different processes can be responsible for vanishing of K_2CO_3 from the samples at high temperatures. Whatever the mechanism, the additive is eliminated after the sintering step, providing nearly pure calcium cobaltite thermoelectric ceramics. Thus, in this approach, potassium carbonate acts rather as a transient liquid phase, providing benefits

of this sintering method, while avoiding the contamination of samples, which can be detrimental for their thermoelectric performance.

The results of powder XRD analysis of all samples after the sintering step, presented in Fig. 4, reveal the main peaks of $Ca_3Co_4O_9$ phase [24]. Traces of the $Ca_3Co_2O_6$ secondary phase were also identified in all the patterns, with peaks at around 20, 32, and 34 degrees (marked by * in Fig. 4a) [25]. Its presence can be attributed to the specifics of the solid state route and to the selective leaching of the calcium cations by liquid K_2CO_3 phase with strong basic character, resulting in minor compositional inhomogeneites in the samples. No shift of diffraction peaks, independently of potassium content was observed for the main phase, suggesting that, if any, the impact of the latter on the crystal lattice and unit cell size is negligible.

Representative SEM micrographs, obtained on longitudinal polished sections of the different samples, are presented in Fig. 5. The traces of $Ca_3Co_2O_6$, indicated by arrows, can be identified by their shape and minor contrast difference with the main phase. The presence of this phase is in agreement with the XRD results previously discussed. The images suggest an apparent trend for decreasing porosity from the pure sample to the one nominally containing 5 wt.% K_2CO_3, followed by a slight increase for 10 wt.% K_2CO_3. The measured density of these samples was 3.37, 3.74, and 3.51 g/cm^3, respectively, with a maximum standard error of 0.03 in all cases. These values roughly correspond to 72, 80, and 75 % of the theoretical density, respectively, and are totally consistent with the SEM observations.

Fig. 6 presents the temperature dependence of electrical resistivity for all samples. The resistivity shows a trend to decrease when temperature raises

(dρ/dT < 0) up to around 400 ºC, indicating a semiconducting-like behaviour. At higher temperatures the samples demonstrate a metallic-like one (dρ/dT > 0). This evolution of electrical resistivity is in agreement with the typically observed in similar materials prepared through the solid state route [26]. Corresponding change in electrical transport behaviour was ascribed to prevailing small-polaron hopping conduction at low temperatures, while mobile charge carriers at higher temperatures are itinerant holes [27]. The samples containing K_2CO_3 additive show 45-75 % lower resistivity than pure $Ca_3Co_4O_9$, being most likely a result of better connectivity between the grains promoted by liquid phase sintering. The higher resistivity found in 10 wt.% K_2CO_3 containing samples can be, at least, partially attributed to their higher porosity. However, it should be noticed that the correlation between sample porosity and the grains connectivity may be quite complex, especially if considering specific bonding, promoted by liquid phase sintering. The minimum values measured at room temperature and 800 ºC for the 5 wt.% K_2CO_3 samples (around 11 and 12 mΩ cm, respectively) are much lower than those obtained in classically sintered materials (~ 33 and 40 mΩ cm, respectively) [7]. Furthermore, they are relatively close to the values measured in high-density textured materials, produced by the hot-pressing technique, determined in the ab direction (8, and 6 mΩ cm at RT and 600 ºC, respectively) [20], or SPS and measured in the same direction (about 5, and 6 mΩ cm at RT and 800 ºC, respectively) [28]. On the other hand, they are lower than measured for the same SPS samples along the c direction (~ 26 and 16 mΩ cm at RT and 800 ºC, respectively) [28].

Fig. 7 shows the variation of Seebeck coefficient with temperature for all the samples. In the graph, it can be clearly seen that the sign of *S* is positive for the

entire measured temperature range, confirming a dominant p-type conduction mechanism. At low temperatures the *S* values are higher for the pure $Ca_3Co_4O_9$ samples, which is in agreement with their higher electrical resistivity. Surprisingly, the largest S at higher temperatures was observed for samples with K_2CO_3 addition, reaching ~ 230 μV/K at 800 ºC. This value is higher than that obtained in hot pressed textured materials in the ab direction (about 175 μV/K at 600 ºC) [20], and SPS textured samples at the same temperature, measured in the ab and the c directions, around 150 and 165 μV/K at 800 ºC, respectively [28]. At the same time, it is only slightly higher than that obtained for solid state sintered materials (~ 200 μV/K) at the same temperature [29]. However, even considering a certain discrepancy of the literature data, the S values, measured in the present work, are the highest ever reported for similar materials. Although the reasons for such large Seebeck coefficient, observed for K_2CO_3–containing samples, are not yet clear, this finding is critically important in the light of seeking highly-performing $Ca_3Co_4O_9$-based thermoelectrics. As Seebeck coefficient, being an intrinsic property of the material, is usually not affected by any microstructural features, possible effects from minor residual fraction of potassium cations in the sample cannot be excluded. These effects are rather relevant when the charge transport is determined by itinerant holes, as suggested by similar temperatures of Seebeck crossover for different samples (Fig. 7) and observed change in resistivity behaviour with temperature. As the increase in *S* values at high temperatures for K_2CO_3–containing samples is significant, the incorporation of potassium cations into the crystal structure of $Ca_3Co_4O_9$ with various impacts on the electronic structure near Fermi level may be rather expected than the formation of minor separate phases.

The temperature dependence of κ for all samples is illustrated in Fig. 8a. All materials show similar thermal conduction behaviour, and κ decreases with the temperature, being consistent with literature data [30,31]. Generally, κ can be expressed as $\kappa = \kappa_l + \kappa_e$, where κ_l is the lattice thermal conductivity contribution and κ_e is the electronic counterpart. κ_e can be estimated from the Wiedemann-Franz's law [32], which is expressed as $\kappa_e = L\,\sigma\,T$, where *L, and* σ are Lorentz number (2.45×10^{-8} V^2/K^2), and electrical conductivity, respectively. Using this expression, κ_e has been calculated in the same temperature range used for the κ measurements. The obtained results, as a function of temperature, are presented in Fig. 8b. The total thermal conductivity of K_2CO_3-containing samples is slightly higher than the measured in pure Ca_3CoO_4. The observed difference is mainly determined by the electronic contributions to the thermal conductivity, with the highest value for the 5 wt.% K_2CO_3–containing material (Fig. 8b) as a result of the better interconnectivity between the grains promoted by the liquid phase sintering process. At the same time, the estimated lattice contribution, κ_l, remains similar for all the samples. It should be noticed that electronic properties, like S, should be more sensitive to the possible incorporation of potassium into the crystal lattice than the lattice thermal conductivity, justified by the very small expected substitution level, and quite close atomic weights of K, Ca and Co, suggesting negligible contribution from mass-difference impurity scattering. On the other hand, the measured κ values at room temperature ($\sim$ 1.3 W/K m) are much lower than those obtained for SPS sintered samples (about 2.4 W/K m) [33], or solid-state sintered materials pressed at 3 GPa (around 2.9 W/K m) [30,31]. The low κ values, observed in

this work, are believed to be mainly a result of relatively high porosity, which decreases the bulk thermal conductivity.

Based on the electrical properties results and κ, it is possible calculating ZT for all the samples; the results are shown in Fig. 9a. It should be noticed that oxide thermoelectrics are rather prospective for high-temperature applications, where their thermoelectric properties become reasonable. In the present work, the thermal conductivity measurements were limited to a low temperature range, due to the equipment limitations. Thus, although ZT values, shown in Fig. 9a, seem to be low, they allow comparing the relevant effects coming from the transient liquid phase sintering. The highest thermoelectric performance is observed for the 5 wt.% K_2CO_3 samples. It should be highlighted that for the discussed temperature range, ZT values follow the same trends observed for the electrical resistivity, namely, increasing from the pure $Ca_3Co_4O_9$ samples to those with 5 wt.% K_2CO_3, and slightly decreasing for the 10 wt.% K_2CO_3 ones.

To evaluate the prospects of the prepared materials in relevant operation conditions ZT values have been estimated at different temperatures (600, 700 and 800 ºC), using the measured electrical resistivity and Seebeck coefficient data, and assuming that the thermal conductivity would remain unchanged from its value at 140 ºC. As the thermal conductivity of $Ca_3Co_4O_9$ compound normally decreases with the temperature, this assumption will allow predicting minimal attained ZT value, while the realistic ones for these conditions should be even higher. These estimations are presented in Fig. 9b, together with the values from previous works [7,20,33]. As it can be observed in the figure, these estimations are fairly higher than the obtained in $Ca_3Co_4O_9$ materials produced by solid state sintering (~ 0.075 at 600 ºC) [20], SPS (about 0.17 at 700 ºC) [33],

or by hot pressing and measured parallel (around 0.07 at 600 ºC) and perpendicular (~ 0.17 at 600 ºC) to the applied load [7]. Moreover, the maximum estimated ZT value at 800 ºC, 0.35 for the 5 wt.% K_2CO_3–containing samples, is nearly twice than the obtained in the pure ones.

Finally, the observed thermoelectric performance of the calcium cobaltite, prepared using 5 wt.% K_2CO_3 additive, suggest good prospects for further improvements in relevant properties of this material, aiming high-temperature applications. The attained benefits are believed to be a result of enhanced interconnectivity of grains, promoted by the sintering approach. Noteworthy that this work was rather focused on demonstrating the advantages of the proposed approach, while several questions, including the reasons for the high Seebeck coefficient, thermal conductivity at high temperatures and possible presence of a minor potassium fraction in the crystal lattice still should be addressed. It is also very important to highlight that the liquid phase effectively disappears (transient liquid phase) after the sintering procedure, thus avoiding possible negative effects on the bulk material.

4. Conclusions

$Ca_3Co_4O_9$ thermoelectric materials were prepared by the classical solid state method with different weight % K_2CO_3 additions (0, 5, and 10). It has been found that K_2CO_3 drastically improves the sintering procedure, modifying the samples density. The additive effectively disappears after sintering, avoiding negative effects on the thermoelectric properties. Combined XRD/SEM studies have shown that all samples possess the $Ca_3Co_4O_9$ phase as the major one, independently of the starting composition. Electrical resistivity was greatly

decreased by K_2CO_3 addition, compared with the pure sample, due to the improvement in grains connectivity. The lattice thermal conductivity was found to be similar for all studied compositions, while the electronic counterpart was responsible for the slightly higher total thermal conductivity of K_2CO_3 containing samples. The best ZT value, estimated at 800 ºC, assuming that the thermal conductivity remains unchanged from 140 ºC, is 0.35 for samples with 5 wt.% K_2CO_3 addition. The estimated results for these samples are significantly higher than the obtained in highly dense textured materials prepared by hot pressing or SPS at the same temperature. The results clearly demonstrated that the transient liquid phase sintering process is a promising route for producing highly-performing $Ca_3Co_4O_9$-based thermoelectrics with relatively high porosity to control thermal conductivity. Finally, it is important to highlight that this process can be extended to any type of ceramic material when choosing the adequate additive composition.

Acknowledgements

The authors wish to thank the MINECO-FEDER (MAT2013-46505-C3-1-R) and Gobierno de Aragón-Fondo Social Europeo (Research Groups T12 and T87) for financial support. The technical contributions of C. Estepa and C. Gallego are also acknowledged. This research was also partially supported by FCT, Portugal (IF/00302/2012 and PEst-C), project RECI/CTM-CER/0336/2012 co-financed by FEDER, QREN reference COMPETE: FCOMP-01-0124-FEDER-027465, and the projects financed by national funds through the FCT/MEC: UID/CTM/50025/2013, UID/CTM/50011/2013.

References

[1] I. Terasaki, Y. Sasago, K. Uchinokura, Large thermoelectric power in $NaCo_2O_4$ single crystals, Phys. Rev. B 56 (1997) R12685-R12687.

[2] N. Sun, S. T. Dong, B. B. Zhang, Y. B. Chen, J. Zhou, S. T. Zhang, Z. B. Gu, S. H. Yao, Y. F. Chen, Intrinsically modified thermoelectric performance of alkaline-earth isovalently substituted $[Bi_2AE_2O_4][CoO_2]_y$ single crystals, J. Appl. Phys. 114 (2013) 043705.

[3] A. Sotelo, G. Constantinescu, Sh. Rasekh, M. A. Torres, J. C. Diez, M. A. Madre, Improvement of thermoelectric properties of $Ca_3Co_4O_9$ using soft chemistry synthetic methods, J. Eur. Ceram. Soc. 32 (2012) 2415-2422.

[4] A. Maignan, D. Pelloquin, S. Hebert, Y. Klein, M. Hervieu, Thermoelectric power in misfit cobaltites ceramics: optimization by chemical substitutions, Bol. Soc. Esp. Ceram. V. 45 (2006) 122-125.

[5] G. Constantinescu, M. A. Torres, Sh. Rasekh, P. Bosque, M. A. Madre, J. C. Diez, A. Sotelo, Thermoelectric properties in $Ca_3Co_{4-x}Mn_xO_y$ ceramics, Adv. Appl. Ceram. 114 (2015) 303-308.

[6] M. M. Seabaugh, I. H. Kerscht, C. L. Messing, Texture development by template grain growth in liquid-phase-sintered alpha-alumina, J. Am. Ceram. Soc. 80 (1997) 1181–1188.

[7] H. Wang, X. Sun, X. Yan, D. Huo, X. Li, J.-G. Li, X. Ding, Fabrication and thermoelectric properties of highly textured $Ca_9Co_{12}O_{28}$ ceramic, J. Alloys Compd. 582 (2014) 294-298.

[8] S. Butt, Y.-C. Liu, J.-L. Lan, K. Shehzad, B. Zhan, Y. Lin, C. W. Nan, High-temperature thermoelectric properties of La and Fe co-doped Ca–Co–O misfit-

layered cobaltites consolidated by spark plasma sintering, J. Alloys Compd. 588 (2014) 277-283.

[9] A. Sotelo, E. Guilmeau, Sh. Rasekh, M. A. Madre, S. Marinel, J. C. Diez, Enhancement of the thermoelectric properties of directionally grown Bi–Ca–Co–O through Pb for Bi substitution, J. Eur. Ceram. Soc. 30 (2010) 1815-1820.

[10] N. M. Ferreira, Sh. Rasekh, F. M. Costa, M. A. Madre, A. Sotelo, J. C. Diez, M. A. Torres, New method to improve the grain alignment and performance of thermoelectric ceramics, Mater. Lett. 83 (2012) 144-147.

[11] M. Mora, A. Sotelo, H. Amaveda, M. A. Madre, J. C. Diez, L. A. Angurel, G. F. de la Fuente, Ag addition effect on laser textured Bi-2212 samples, Bol. Soc. Esp. Ceram. V. 44 (2005) 199-203.

[12] F. Kahraman, M. A. Madre, Sh. Rasekh, C. Salvador, P. Bosque, M. A. Torres, J. C. Diez, A. Sotelo, Enhancement of mechanical and thermoelectric properties of $Ca_3Co_4O_9$ by Ag addition, J. Eur. Ceram. Soc. 35 (2015) 3835-3841.

[13] B. C. Zhao, Y. P. Sun, W. H. Song, Magnetic and transport properties in the Ti doped cobaltite $Ca_3Co_{4-x}Ti_xO_9$ ($0 \leq x \leq 0.8$) single crystals, J. Appl. Phys. 99 (2006) 073906.

[14] S. Bhattacharya, D. K. Aswal, A. Singh, C. Thinaharan, N. Kulkarni, S. K. Gupta, J. V. Yakhmi, Anisotropic electrical transport studies of $Ca_3Co_4O_9$ single crystals grown by the flux method, J. Cryst. Growth 277 (2005) 246-251.

[15] C. R. Hammond, Handbook of Physics and Chemistry, 90th ed., CRC Press: Boca Raton, Fl, 2009.

[16] A. Sotelo, Sh. Rasekh, M. A. Torres, P. Bosque, M. A. Madre, J. C. Diez. Effect of synthesis methods on the $Ca_3Co_4O_9$ thermoelectric ceramic performances, J. Solid State Chem. 221 (2015) 247-254.

[17] Sh. Rasekh, M. A. Torres, G. Constantinescu, M. A. Madre, J. C. Diez, A. Sotelo, Effect of Cu by Co substitution on $Ca_3Co_4O_9$ thermoelectric ceramics, J. Mater. Sci.: Mater. Electron. 24 (2013) 2309-2314.

[18] M. A. Madre, F. M. Costa, N. M. Ferreira, A. Sotelo, M. A. Torres, G. Constantinescu, Sh. Rasekh, J. C. Diez, Preparation of high-performance $Ca_3Co_4O_9$ thermoelectric ceramics produced by a new two-step method, J. Eur. Ceram. Soc. 33 (2013) 1747-1754.

[19] N. Prasoetsopha, S. Pinitsoontorn, T. Kamwanna, V. Amornkitbamrung, K. Kurosaki, Y. Ohishi, H. Muta, S. Yamanaka, The effect of Cr substitution on the structure and properties of misfit-layered $Ca_3Co_{4-x}Cr_xO_{9+\delta}$ thermoelectric oxides, J. Alloys Compd. 588 (2014) 199-205.

[20] D. Kenfaui, B. Lenoir, D. Chateigner, B. Ouladdiaf, M. Gomina, J. G. Noudem, Development of multilayer textured $Ca_3Co_4O_9$ materials for thermoelectric generators: influence of the anisotropy on the transport properties, J. Eur. Ceram. Soc. 32 (2012) 2405-2414.

[21] R. M. German, P. Suri, S. J. Park, Review: Liquid phase sintering, J. Mater. Sci. 44 (2009) 1-39.

[22] R. L. Lehman, J. S. Gentry, N. G. Glumac, Thermal stability of potassium carbonate near its melting point, Thermochim. Acta 316 (1998) 1-9.

[23] K. Sugiura, M. Yamauchi, K. Tanimoto, Y. Yoshitani, Evaluation of volatile behaviour and the volatilization volume of molten salt in DIR-MCFC by using the image measurement technique, J. Power Sources 145 (2005) 199-205.

[24] C. Brisi, P. Rolando, The calcium oxide-cobalt (II) oxide-oxygen system, Ann. Chim. (Rome) 58 (1968) 676-683.

[25] E. Woermann, A. Muan, Phase equilibria in the system CaO-cobalt oxide in air, J. Inorg. Nucl. Chem. 32 (1970) 1455-1459.

[26] G. Constantinescu, Sh. Rasekh, M. A. Torres, J. C. Diez, M. A. Madre, A. Sotelo, Effect of Sr substitution for Ca on the $Ca_3Co_4O_9$ thermoelectric properties, J. Alloys Compd. 577 (2013) 511-515.

[27] M. Schrade, H. Fjeld, T. G. Finstad, T. Norby, Electronic transport properties of $[Ca_2CoO_{3-\delta}]_q[CoO_2]$, J. Phys. Chem. C 118 (2014) 2908-2918.

[28] N. Y. Wu, T. C. Holgate, N. V. Nong, N. Pryds, S. Linderoth, High temperature thermoelectric properties of $Ca_3Co_4O_{9+\delta}$ by auto-combustion synthesis and spark plasma sintering, J. Eur. Ceram. Soc. 34 (2014) 925-931.

[29] Sh. Rasekh, M. A. Torres, G. Constantinescu, M. A. Madre, J. C. Diez, A. Sotelo, Effect of Cu by Co substitution on $Ca_3Co_4O_9$ thermoelectric ceramics, J. Mater. Sci.: Mater. Electron. 24 (2013) 2309-2314.

[30] L. Xu, F. Li, Y. Wang, High-temperature transport and thermoelectric properties of $Ca_3Co_{4-x}Ti_xO_9$, J. Alloys Compd. 501 (2010) 115-119.

[31] Y. Zhang, J. Zhang, Rapid reactive synthesis and sintering of textured $Ca_3Co_4O_9$ ceramics by spark plasma sintering, J. Mater. Process. Technol. 208 (2008) 70-74.

[32] M. E. Fine, N. Hsieh, Wiedermann-Franz-Lorenz relation in highly electronic-conducting oxides, J. Am. Ceram. Soc. 57 (1974) 502-503.

[33] R. Tian, T. Zhang, D. Chu, R. Donelson, L. Tao, S. Li, Enhancement of high temperature thermoelectric performance in Bi, Fe co-doped layered oxide-based material $Ca_3Co_4O_{9+\delta}$, J. Alloys Compd. 615 (2014) 311-315.

Figure captions

Figure 1. Scheme of the sintering process using potassium carbonate as an additive for liquid phase sintering.

Figure 2. Representative TEM micrograph of $Ca_3Co_4O_9$ + 5 wt.% K_2CO_3 sample (a). EDS mapping of calcium (b), cobalt (c) and potassium (d) in the same region.

Figure 3. a) SEM micrograph of the alumina powder bed after samples sintering with potassium carbonate: #1 corresponds to the area under the sintered sample, and #2 and #3 are the areas with increasing distance from the sample. b) EDS spectrum, taken in the area #1 without Ca or Co traces.

Figure 4. Room-temperature powder XRD patterns of pure $Ca_3Co_4O_9$ (a), and samples containing 5 (b) and 10 (c) wt.% K_2CO_3 additive. Diffraction planes indicate the $Ca_3Co_4O_9$ phase, "*" mark shows the peaks corresponding to the $Ca_3Co_2O_6$ phase, and # identifies the (111) reflection of Si used as internal reference.

Figure 5. Representative SEM micrographs of polished sections of $Ca_3Co_4O_9$ + x wt.% K_2CO_3 samples, for x= 0 (a), 5 (b), and 10 (c). Arrows indicate the $Ca_3Co_2O_6$ phase with very similar contrast to $Ca_3Co_4O_9$ one but different shape.

Figure 6. Electrical resistivity evolution with temperature for $Ca_3Co_4O_9$ + x wt.% K_2CO_3 samples with x= (●) 0, (■) 5, and (◆) 10.

Figure 7. Seebeck coefficient evolution with temperature for $Ca_3Co_4O_9$ + x wt.% K_2CO_3 samples with x= (●) 0, (■) 5, and (◆) 10.

Figure 8. a) Total thermal conductivity; and b) Electronic contribution to the thermal conductivity vs. temperature. Symbols denote the different $Ca_3Co_4O_9$ + x wt.% K_2CO_3 samples for x= (●) 0, (■) 5, and (◆) 10.

Figure 9. ZT vs. temperature of $Ca_3Co_4O_9$ + x wt.% K_2CO_3 samples for x= (●) 0, (■) 5, and (◆) 10. a) calculated; b) estimated values at high temperatures and compared with literature data ◣ [7]; ▲ [20]; and ▼ [33].

Table 1. Atomic % evolution determined by EDS in the three different zones observed in the alumina bed.

Zone	K (at. %)	Al (at. %)
1	48	52
2	35	65
3	22	78

Figure 1

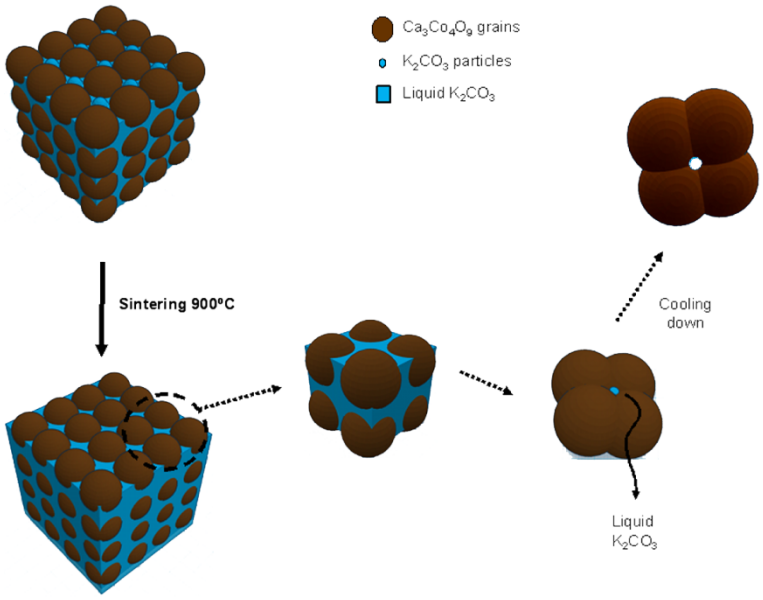
$Ca_3Co_4O_9$ grains
K_2CO_3 particles
Liquid K_2CO_3
Sintering 900°C
Cooling down
Liquid K_2CO_3

Figure 2

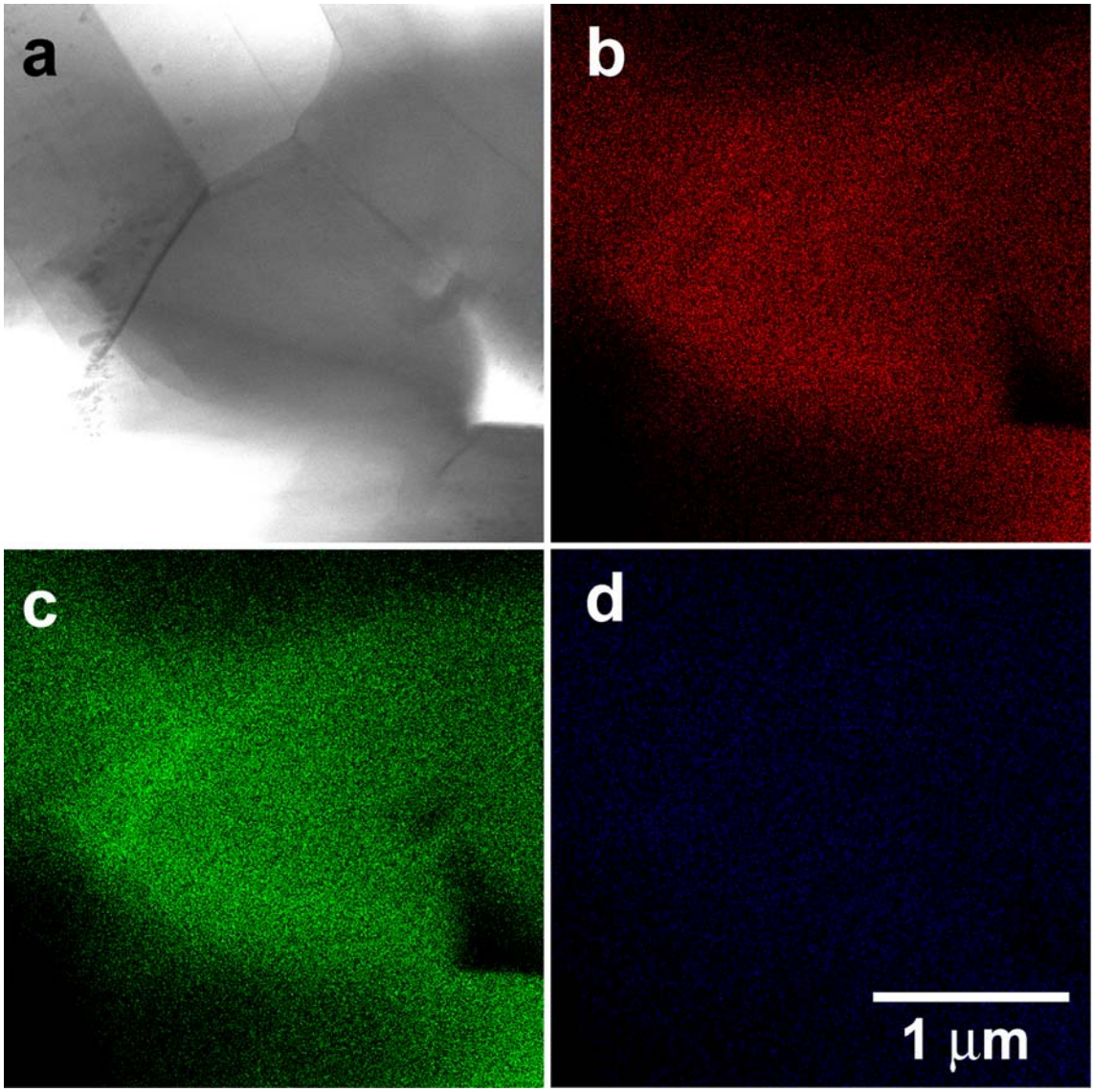

Figure 3

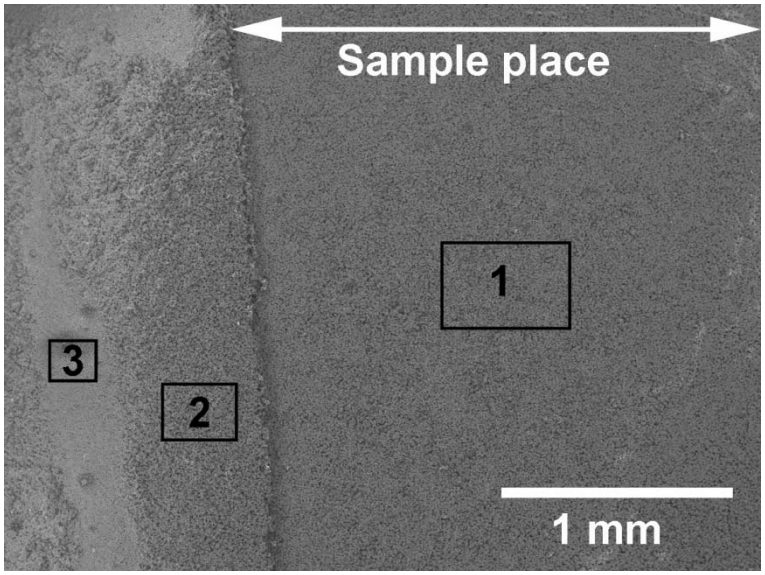

Figure 4

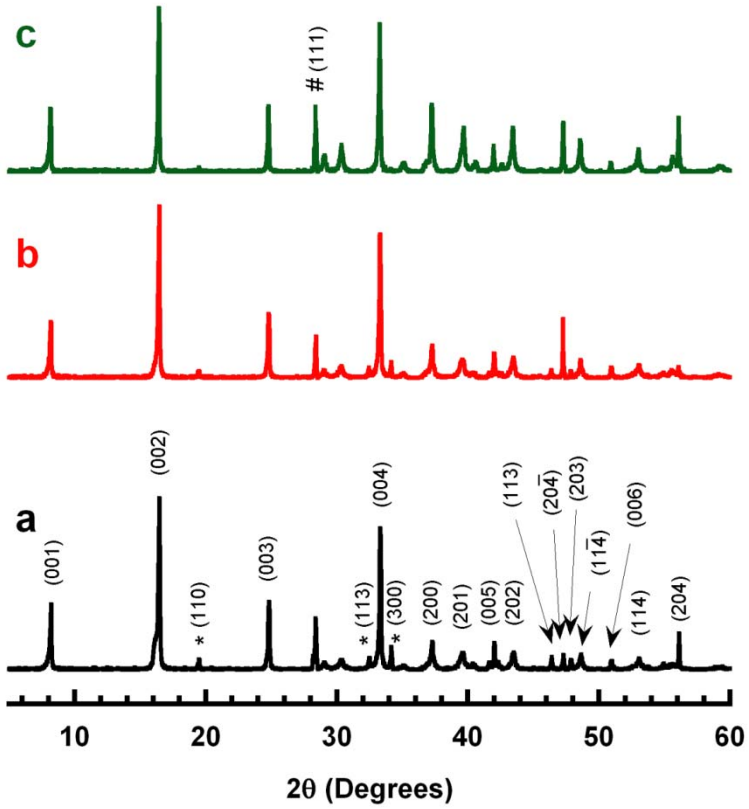
c
(111)
b
a
(001)
(002)
* (110)
(003)
* (113)
(004)
* (300)
(200)
(201)
(005)
(202)
(113)
(20$\bar{4}$)
(203)
(11$\bar{4}$)
(006)
(114)
(204)
10
20
30
40
50
60
2θ (Degrees)

Figure 5

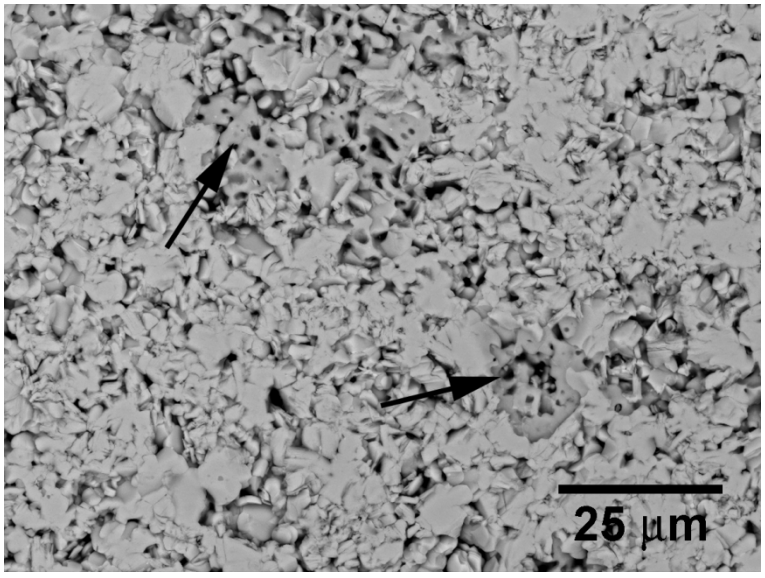

Figure 6

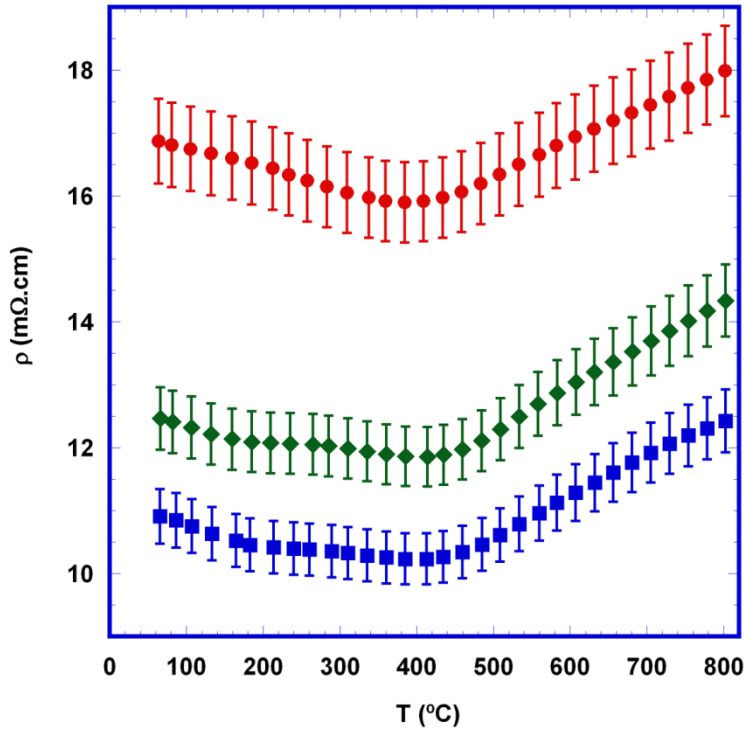

Figure 7

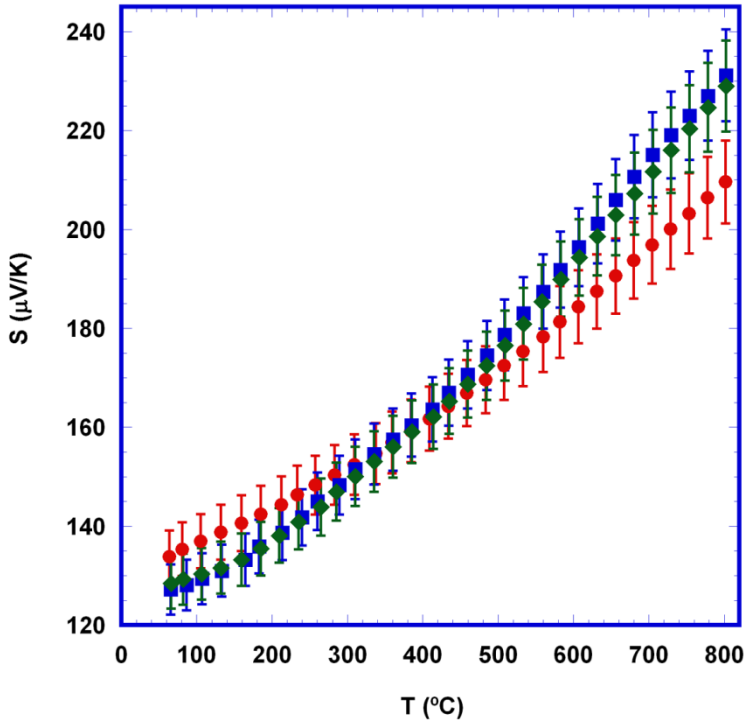
240
220
200
180
160
140
120
S (μV/K)
0
100
200
300
400
500
600
700
800
T (°C)

Figure 8

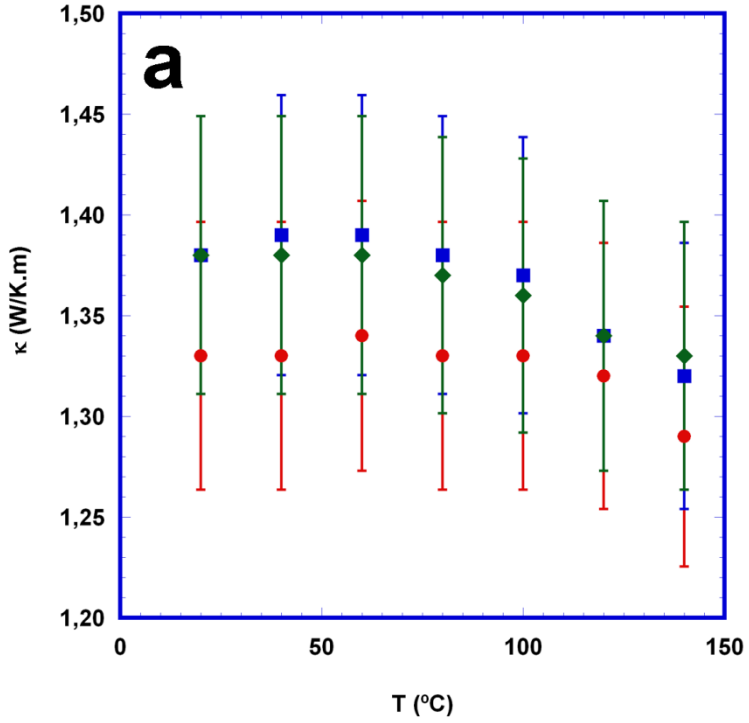
a
1,50
1,45
1,40
1,35
1,30
1,25
1,20
κ (W/K.m)
0
50
100
150
T (°C)

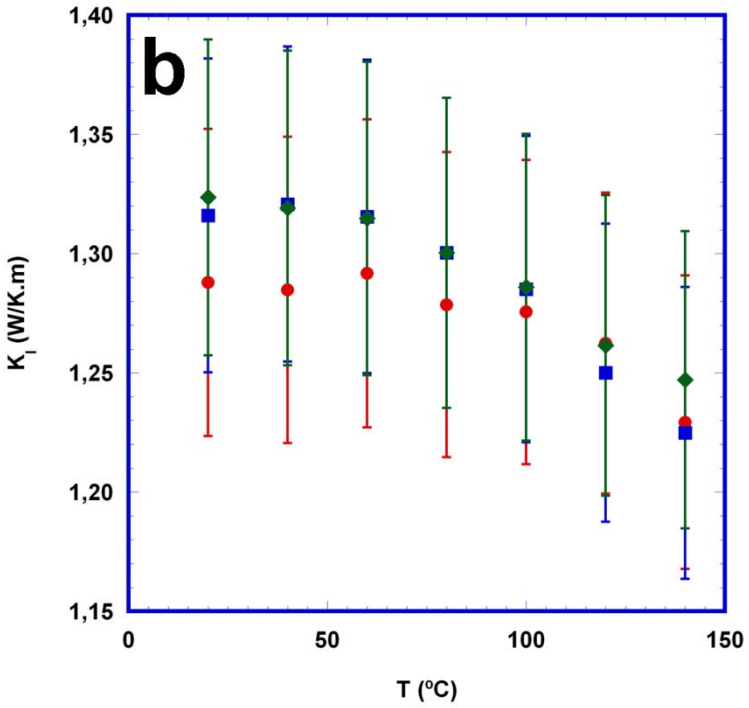
b
1,40
1,35
1,30
1,25
1,20
1,15
K_l (W/K.m)
0
50
100
150
T (°C)

Figure 9

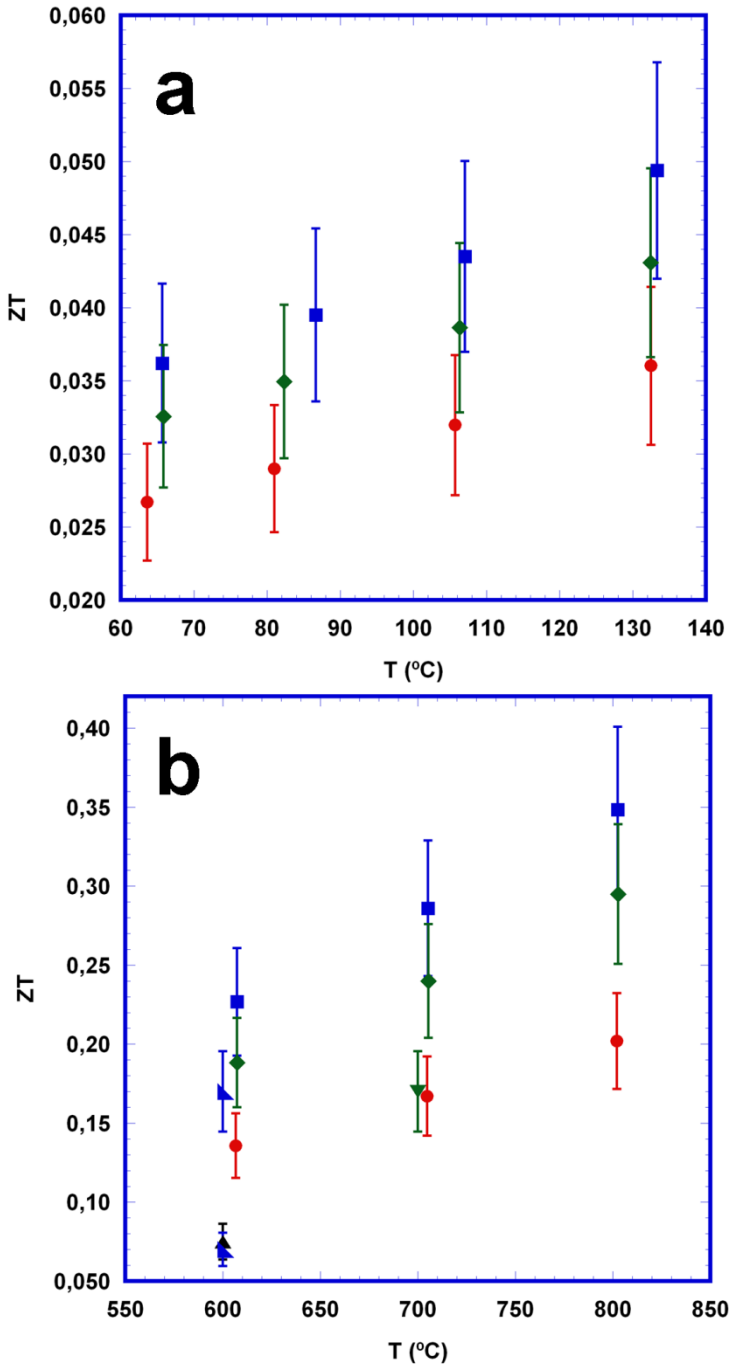
a
ZT
0,060
0,055
0,050
0,045
0,040
0,035
0,030
0,025
0,020
60
70
80
90
100
110
120
130
140
T (°C)
b
ZT
0,40
0,35
0,30
0,25
0,20
0,15
0,10
0,050
550
600
650
700
750
800
850
T (°C)